Title

A sloped piecemeal Gaussian model for characterising foveal pit shape

Journal

Ophthalmic & Physiological Optics, 36(6)

ISSN

0275-5408

Authors

Liu, Lei
Marsh-Tootle, Wendy
Harb, Elise N
et al.

Publication Date

2016-11-01

DOI

10.1111/opo.12321

Peer reviewed

HHS Public Access

Author manuscript

Ophthalmic Physiol Opt. Author manuscript; available in PMC 2020 February 18.

Published in final edited form as:

Ophthalmic Physiol Opt. 2016 November ; 36(6): 615–631. doi:10.1111/opo.12321.

A sloped piecemeal Gaussian model for characterising foveal pit shape

Lei Liu[1], **Wendy Marsh-Tootle**[1], **Elise N. Harb**[2], **Wei Hou**[3], **Qinghua Zhang**[3], **Heather A. Anderson**[4], **Thomas T. Norton**[1], **Katherine K. Weise**[1], **Jane E. Gwiazda**[5], **Leslie Hyman**[3], **COMET Group**[1,3,4,5]

[1]School of Optometry, University of Alabama at Birmingham, Birmingham

[2]School of Optometry, University of California at Berkeley, Berkeley

[3]Family, Population and Preventive Medicine, Stony Brook Medicine, New York

[4]College of Optometry, University of Houston, Houston

[5]New England College of Optometry, Boston, USA

Abstract

Purpose: High-quality optical coherence tomography (OCT) macular scans make it possible to distinguish a range of normal and diseased states by characterising foveal pit shape. Existing mathematical models lack the flexibility to capture all known pit variations and thus characterise the pit with limited accuracy. This study aimed to develop a new model that provides a more robust characterisation of individual foveal pit variations.

Methods: A Sloped Piecemeal Gaussian (SPG) model, consisting of a linear combination of a tilted line and a piecemeal Gaussian function (two halves of a Gaussian connected by a separate straight line), was developed to fit retinal thickness data with the flexibility to characterise different degrees of pit asymmetry and pit bottom flatness. It fitted the raw pit data between the two rims of the fovea to improve accuracy. The model was tested on 3488 macular scans from both eyes of 581 young adults (376 myopes and 206 non-myopes, mean (S.D.) age 21.9 (1.4) years). Estimates for retinal thickness, wall height and slope, pit depth and width were derived from the best-fitting model curve. Ten variations of Gaussian and Difference of Gaussian models were fitted to the same scans and compared with the SPG model for goodness of fit (by Root mean square error, RMSE), model complexity (by the Bayesian Information Criteria) and model fidelity.

Results: The SPG model produced excellent goodness of fit (mean RMSE = 4.25 and 3.89 μm; 95% CI: 4.20, 4.30 and 3.86, 3.93 for fitting horizontal and vertical profiles respectively). The SPG model showed pit asymmetry, with average nasal walls 17.6 (11.6) μm higher and 0.96 (0.61)° steeper than temporal walls and average superior walls 7.0 (12.2) μm higher and 0.41 (0.65)° steeper than the inferior walls. The SPG model also revealed a continuum of human foveal shapes, from round bottoms to extended flat bottoms (up to 563 μm). 49.1% of foveal profiles

Correspondence: Lei Liu, liul7788@uab.edu.

Disclosure

The authors report no conflicts of interest and have no proprietary interest in any of the materials mentioned in this article.

were best fitted with a flat bottom >30 μm wide. Compared with the other tested models, the SPG was the preferred model overall based on the Bayesian Information Criteria.

Conclusions: The SPG is a new parsimonious mathematical model that improves upon other models by accounting for wall asymmetry and flat pit bottoms, providing an excellent fit and more faithful characterisation of typical foveal pit shapes and their known variations. This new model may be helpful in distinguishing normal foveal shape variations by refractive status as well by other characteristics such as sex, ethnicity and age.

Keywords

foveal pit; human retina; mathematical model; optical coherence tomography

Introduction

The shape of the foveal pit, because of its unique morphology, histological composition and functional importance, has been the focus of many studies. Visual function measures such as resolution acuity and contrast sensitivity have been related to the foveal pit shape.[1-5] Individual foveal pit development begins with a narrow and deep prenatal fovea and ends with a wider and shallower adult fovea due to the rapid ocular growth after birth.[6-11] Interest in quantitative characterisation of foveal pit shape has grown recently due to the advancement of the optical coherence tomography (OCT) technology that allows non-invasive imaging of the retina at unprecedented resolution and accuracy. This new technology has made it possible to obtain high-quality macular scans from individuals in different populations with and without ocular disease and from repeated scans on the same subject at different points over time. This has created new opportunities to enhance understanding of individual development of the fovea, its normal variations and the relationships between foveal shape and various ocular and neurological diseases. Recent studies based on large sample sizes have described macular morphologies in populations of varying ethnicity, gender and ages, providing normative data for detecting pathological changes.[12-24] As an example of the many applications of OCT in eye care, the epidemic of myopia in Asia[25] and the increasing risk of macular abnormalities associated with high myopia[26] have led to many OCT studies seeking to evaluate the relationship between macular morphology and myopia severity, to determine whether this relationship varies in different gender and ethnic groups and to identify macular features that may indicate risk of myopia-related retinal pathologies.[27-39]

Compared to the fast increase in quality and availability of OCT scans, the development of automated methods to quantitatively characterise foveal morphology with minimal operator intervention has lagged behind. The most popular method is the Early Treatment Diabetic Retinopathy Study macular thickness map, in which retinal thickness measures in the nine zones of a fixed grid are averaged to form a rudimentary map. It is known that averaging retinal thickness across large zones conceal indicative foveal features (e.g. pit wall slopes and bottom shapes) and that imposing a fixed grid on foveas with large known variances in width and thicknesses is likely to introduce large measurement variance. Nevertheless, this map was still used in most studies concerning macular morphology, including all the OCT articles cited above. A more powerful strategy to achieve quantitative assessment is to derive

mathematical representations of the foveal pit from raw OCT data. These mathematical representations can then be used to provide much richer, more quantitative and individualised characterisation of the fovea and thus can help to differentiate subtler differences among normal populations and to detect smaller pathological changes of the fovea.

Two approaches have been used to generate mathematical representations of the foveal pit. The data-driven approach used a generic spline function or a combination of mathematical operators determined by symbolic regression to generate best-fitting curves to OCT foveal profiles and derives pit parameters from these curves.[40-42] The model-driven approach represented prior knowledge about the fovea, i.e., 'prototype foveal pit', with a mathematical function (a model) and a fixed set of model coefficients, fitted the model to OCT data, extracted foveal landmarks directly from the best-fitting model coefficients and derived foveal pit characterisations from the landmarks.[43-49]

The model-driven approach has been successfully used to study the normal foveal pit variation with race and gender,[46] the relationship between pit shape and foveal avascular zone,[47] and the foveal abnormalities in oligocone trichromacy,[50] amblyopia,[44] albinism[48] and Parkinson's disease.[51] However, existing models can adequately characterise some foveal pits, but not all. Specifically, some models do not take the asymmetry of the pit into consideration (blue dashed curve in Figure 1) and may misfit those pits that have extended flat bottoms (red solid curve in Figure 1). A more accurate characterisation of all foveal pits thus requires flexibilities to fit asymmetric pits with different bottom shapes. Another limitation of previous modelling approaches is their use of either all the A-scans[43,44,46] or the A-scans within a fixed distance (1.25 or 2.5 mm) from an estimated pit centre.[45,51] We speculate that including parafoveal data into the fitting process may compromise the accuracy of curve fitting inside the pit itself.

To address limitations of existing modelling efforts, we developed a new mathematical model that can more accurately and reliably characterise a wider range of foveal pit shapes. We also determined the relative merits (goodness of fit, model complexity and model fidelity) of the new model with several variations of the Gaussian and the Difference of Gaussians (DoG) models using the same set of scan data. These were accomplished by fitting data from a set of OCT macular scans obtained from a group of ethnically diverse young adult myopes and non-myopes from the Correction of Myopia Evaluation Trial (COMET) study, at their 12th year COMET visits.

Methods

Subjects

In this study, Spectral Domain OCT (http://www.optovue.com - note that the device used in the study, RTVue-100, is no longer in production) macular scans were taken from 376 young myopes and 206 age-, sex-, and ethnicity-matched non-myopes (mean (S.D.) age 21.9 (1.4) years) at four clinical centres (Optometry Schools/Colleges in Birmingham, Alabama, Boston, Massachusetts, Houston, Texas, and Philadelphia, Pennsylvania). Among myopes, 46% were male, 44% were white, 27% African–American, 16% Hispanic, 8% Asian and 5%

mixed. The non-myopes had similar sex and ethnicity profiles. The COMET study and protocols conformed to the Tenets of the Declaration of Helsinki. The research protocols were reviewed and approved by the institutional review boards of each participating institution. Written informed consents were obtained from participants, all of whom were 18 years of age or older at the time these scans were taken.

OCT data

Enhanced Macular Map 5 (EMM5) scans of RTVue were obtained from the right and left eyes of the subjects (1164 eyes). Three high-quality consecutive scans (Signal Strength Index SSI >50, higher than 39, the manufacturer recommended cut off for EMM5) per eye were obtained from 99% (1151) of eyes, with more or fewer scans per eye obtained on the remaining 1%, resulting in a total of 3501 scans. Each scan consisted of 13 horizontal and 13 vertical cross-sectional retinal thickness (the difference between the internal limiting membrane and the retinal pigment epithelium elevations) profiles. Each thickness profile was 803-pixels long, covering a nominal 6 mm distance. A custom computer program was used to automatically search for the profile that had the deepest pit near the middle of the 803-pixel scan among the 13 profiles for both horizontal and vertical directions. One horizontal and one vertical profile were selected from each scan for study.

Data preparation for model fitting

To focus model fitting on the pit, two datasets were extracted from each profile (black curve in Figure 2). This was achieved by first smoothing the profile (100-pixel span smoothing) so that the local minimum near the centre of the smoothed profile and the local maximums on the two sides of the minimum (blue and orange arrows in Figure 2) could be located. A narrow and a wide dataset were created using these landmarks. The *narrow dataset* included only the unsmoothed raw data points between the two local maximums (green curve in Figure 2), thus ignoring the parafoveal data. The mean (S.D.) lengths of the *narrow datasets* were 271 (36) (range from 174 to 390 pixels) and 310 (43) (range from 177 to 450) pixels for vertical and horizontal directions, respectively. The horizontal datasets were longer because the pit in general had a horizontal oval shape. A *wide dataset*, which included the short dataset plus an extra 120 pixels beyond each of the two local maximums (red curve in Figure 2), was created for model comparison. All data points in each profile, whether narrow or wide, were fitted simultaneously.

All data were converted to microns (μm) by applying the nominal scaling factors of 7.5 μm/pixel horizontal and 3 μm/pixel vertical to the raw thickness data to provide more customary units for reporting results. Although it has been shown that axial length can impact OCT feature measurements,[46,52] axial length correction was not critical in this study since we were evaluating model fitting within the same eye rather than comparing features across eyes. It is also known that an artefact may exist in the current OCT display because the displayed orientation of individual A-scans may not always agree with the expected OCT scan paths.[53] However, because the new model was only fitted to the central 1.5–2.25 mm of the scan (narrow dataset), the artefact would have little effect on the pit characterisation accuracy.[53]

Sloped Piecemeal Gaussian (SPG) model

Rationale and equations—A new model, the Sloped Piece Gaussian (SPG), was developed to characterise a prototype foveal pit that had smooth, sigmoidal walls, could be asymmetric on the two sides of the pit and could have a bottom that was not round but flat. The basis of the SPG is a Gaussian function (G).

$$G = e^{-(x-\mu)^2/\sigma^2} \tag{1}$$

The coefficient μ is the location of the centre of the Gaussian function and σ is its standard deviation.

To introduce the flexibility to fit pits with variable extents of flat bottoms, the two halves of the Gaussian function were pulled apart by a distance of λ, and then connected by a straight horizontal line at the top to form a piecemeal Gaussian, $\bar{G}$.

$$\bar{G} = \begin{cases} G & x < \mu - \lambda/2 \\ \max(G) & \mu - \lambda/2 \le x \le \mu + \lambda/2 \\ G & x > \mu + \lambda/2 \end{cases} \qquad (\lambda \ge 0) \tag{2}$$

To introduce a variable degree of asymmetry to the model, a line with a slope of f was added to $\bar{G}$. This function was also flipped vertically to represent a pit. The complete SPG function, specified in Equation 3, has 6 coefficients: μ and g determine the x- and y-locations of the function; σ determines the shape of the walls; f is related to the amount of asymmetry; a determines the depth of the pit and λ is the extent of the flat pit bottom.

$$y = g - (a\bar{G} + fx) \tag{3}$$

Although SPG is a piecemeal function, it is used as a whole when fitting OCT data, with all coefficients determined simultaneously in one fitting procedure.

SPG landmarks

The SPG model produced three pairs of landmarks for each horizontal and vertical profile, (1) two rim points, $\mathscr{R}$ and $\mathscr{R}$', the highest points on the two sides of the pit, (2) two wall points, $\mathscr{W}$ and $\mathscr{W}$', points on the walls of the curve where the slopes were maximum, and (3) two bottom points, $\mathscr{B}$ and $\mathscr{B}$', locations where the walls transit to the flat bottom. Figure 3 shows these landmarks designated by yellow circles, for a sample horizontal profile. Similar landmarks and parameters were determined from fitting the vertical profiles. Because the Gaussian monotonically approached an asymptotic line, $g–fx$ (red line in Figure 3), and thus had no local maximums, the rim points, $\mathscr{R}$ and $\mathscr{R}$', were determined by locating the point where the curve first deviated from the asymptotic line by a preset distance, 0.025 pixels. The *wall points*, $\mathscr{W}$ and $\mathscr{W}$', were determined by the peak and trough locations of the first derivative of the model curve. In scans where the pits have round bottoms, the two bottom

points, $\mathscr{B}$ and $\mathscr{B}$', merge into one, $\mathscr{B}$. In scans where the pits are asymmetric, there is a small *y*-offset between the pairs of corresponding landmarks.

SPG foveal pit parameters

Parameters of pit width and depth, wall heights and slopes and retinal thickness (Figure 3) were computed from the three pairs of landmarks as follows.

1. Pit widths: The top, middle and bottom widths of the pit were defined as the differences between the *x*-coordinates of the rim, wall and bottom point pairs, respectively. If a pit had a truly round bottom, its bottom width was zero. When the pit was asymmetric, the distance between a pair of landmarks, for example, $\mathscr{R}$ and $\mathscr{R}$', was slightly longer than the difference between their *x*-coordinates. However, the difference between the distance and the *x*-coordinate difference was very small (~0.33 μm, averaged across all profiles). Therefore, all pit widths reported herein were the difference between the *x*-coordinates of the corresponding landmarks.
2. Pit wall heights: Local heights of the nasal, temporal, superior and inferior walls of a pit were defined as the *y*-coordinate difference between the corresponding rim and bottom landmarks. These heights were different if the fitting curve was asymmetric.
3. Pit Depth: The pit depth of a foveal profile was defined as the mean of the heights of the opposing walls. Because the pit depths in the horizontal and vertical foveal profiles could differ, pit depth must consider both profiles; therefore, the mean depth of the pit was defined as the mean of depths of the horizontal and vertical profiles of the same eye.
4. Pit wall slopes: The slopes of the nasal, temporal, superior and inferior walls were defined as the maximum slopes on corresponding walls relative to the positive *x*-direction. Only the angle, not the signs of the slopes were considered.
5. Maximum and minimum retinal thickness: The maximum retinal thicknesses on the nasal, temporal, superior and inferior sides of the pit were determined by the *y*-coordinates of the corresponding rim points (measured from the retinal pigment epithelium or $y = 0$). The overall maximum thickness of the fovea was estimated based on the mean of the four local maximum thicknesses. The minimum retinal thickness of a foveal pit was determined by the mean of the *y*-coordinates of all its bottom landmarks.

Model comparisons

In order to assess the relative merits of the SPG model and to achieve a better understanding on model characterisation of the foveal pit, a systematic approach was taken to fit the same macular scan data using the four variations of Gaussian or Difference of Gaussian models described below and to compare their goodness of fit, model complexity and model fidelity. These models permuted the symmetry and bottom shape factors. The effects of dataset width (narrow vs wide) and restricting model coefficient values were also compared.

Models to be compared

Gaussian: A simple Gaussian function (four coefficients, $y = g - aG$, where G is the Gaussian defined in Equation 1).[4]

Sloped Gaussian: A sloped line was added to a symmetric Gaussian function to introduce asymmetry (five coefficients).

Difference of Gaussian (DoG): The difference of two Gaussian functions with their centres aligned ($\Delta\mu = 0$), resulting in a symmetric DoG function with six coefficients.[43]

$$\mathrm{DoG} = g - a[e^{-(x-\mu)^2/\sigma^2} - \mathrm{d}e^{-(x-\mu-\Delta\mu)^2/(e\sigma)^2}] \quad (4)$$

The coefficients d and e in the second Gaussian function were ratios of the amplitudes and the σ's of the first and the second Gaussians. Using ratios was convenient when applying restrictions to the coefficient space of the DoG model. For example, forcing coefficients $d > 1$ and $e < 1$ ensured a 'normal' DoG with two shoulders and one pointed pit and thus eliminated the possibility of the function taking on a shape that does not agree with the prototype shape.

Offset Difference of Gaussian (oDoG): A non-zero x-offset between the centres of the two Gaussians of a symmetric DoG model (Equation 4) was allowed ($\Delta\mu \neq 0$) to produce a seven-coefficient asymmetric offset DoG (oDoG) model.[44] We noticed that when the oDoG coefficients were not restricted, the resultant curve might deviate significantly from the prototype pit shape. An empirical assessment found that restricting $\Delta\mu$ to between −17 and +17 pixels could minimize the deviation.

Extraction of pit landmarks and parameters

These models were built on the assumption that the prototype foveal pit had a round bottom and sigmoidal smooth walls.[4,43,44,46] The method that was used to characterise the pit shape from the best-fitting model coefficients was defined based on this assumption. Specifically, five landmarks were extracted using the first derivative of the best fitting curve, corresponding to its three zero-crossings, one peak and one trough. The two outside zero-crossings were the locations of the two rim points and the zero-crossing in the middle was the location of the pit bottom point. The peak and trough, one on each side of the pit bottom, defined the wall locations that had the maximum slopes. Pit parameters such as the width, depth, minimum and maximum retinal thickness and the heights and slopes of the walls were computed from these five landmarks.[43,44,46] The coherence of the prototype fovea and the foveal landmark extraction method of these models allowed us to judge whether the best-fitting curve generated by a model conformed to the model's prototype fovea. For example, if the first derivative had more than one local peak on one side of the pit bottom, the pit wall on this side could not be sigmoidal, the correct wall landmark could not be correctly extracted and the curve would be considered 'distorted'.

Fitting retinal thickness data (SPG and comparison models)

The SPG model was fitted to the narrow-datasets (Figure 2, green line) to evaluate its goodness of fit and its ability to characterise the foveal pit. Ten additional model fits were performed on the same scans to determine the relative merits of the SPG. Specifically, the Gaussian and sloped Gaussian models were fitted to the narrow dataset without coefficient restriction. The DoG and oDoG models were fitted to both the narrow and the wide datasets (subscripts '*N*' and '*W*') with coefficient space unrestricted (coefficients took any values, subscript '*U*') and restricted (coefficients restricted to $d > 1$, $e < 1$ and $-17 < \Delta\mu < +17$, subscript '*R*'). As an example, $oDoG_{NU}$ was the offset DoG model fit to the narrow dataset with unrestricted coefficient space.

Custom Matlab (http://www.mathworks.com/products/matlab/) programs were developed to perform nonlinear least squares curve fits, extract foveal pit landmarks, compute pit parameters and assess goodness of fit. Fits were performed on raw data. No smoothing or averaging or down-sampling was done to the data before fitting.

Data analysis

Among the 3501 available macular scans, 10 were excluded from analysis because of clear deviations from a normal foveal pit, e.g., a large step in the middle of a pit profile or no obvious pit. The poor quality of these scans was confirmed by comparison with the repeated scans from the same eye. Analyses are based on the 3491 remaining good quality scans. Subtler segmentation errors of the inner limiting membrane and retinal pigment epithelium elevations of these scans were not examined or corrected. When image quality was good (SSI > 39), data accuracy was high. For example, full retinal thickness measures (from inner limiting membrane to the bottom of retinal pigment epithelium) obtained from the EMM5 scans of RTVue-100 had mean intra-eye repeated scan S.D.s < 3 μm.[54,55]

Because the 3491 scans included repeated scans of the same eye and both eyes of the same subject, the fitting outcomes were not independent. To ensure that the correlations among repeated intra-eye and intra-personal scans were taken into account appropriately, the analyses were limited to subjects who had good scan data from both eyes and had at least two repeated scans per eye. Of the 582 subjects, one was excluded because scan data were available in one eye only. This resulted in a total of 3488 good quality scans from both eyes of 581 subjects (1747 right eyes and 1741 left eyes). In addition, each scan had one horizontal and one vertical profile.

The curve fitting was performed on individual profiles, but the fitting results from intra-eye repeated scans was averaged to produce one characterisation of the fovea, resulting in the goodness of fit and pit parameters for 581 pairs of 'foveas'. A set of analyses were conducted to justify averaging results from intra-eye repeated scans. Specifically, there were no statistically significant differences among the root mean squared errors (RMSE) obtained from fitting intra-eye repeated scans ($F_{2,3472} = 0.47$, $p = 0.63$ for vertical; $F_{2,3472} = 0.15$, $p = 0.86$ for horizontal). A set of repeatability analyses (see Repeatability of Foveal Pit Characterisation in Results) also showed that SPG characterisations of repeated scans of the

same eye were highly repeatable. Therefore, unless otherwise indicated, the analyses and discussions were fovea-based, not scan-based.

To account for potential correlations between the two eyes of the same subject, between horizontal and vertical profiles of the same scan or among locations around the same fovea, comparisons of goodness of fit and pit parameters were conducted using a repeated ANOVA, with the Eye (right and left), Direction (horizontal and vertical) or Location (nasal, temporal, superior and inferior) as the within-subject variables.[56] These analyses showed that the two eyes of the subjects were not significantly different in most pit parameters (p-value ranged from 0.095 to 0.46). The only significantly different measure between the two eyes was the minimum retinal thickness ($F_{1,580} = 8.58$, $p = 0.004$), but the magnitude of the difference was only 0.8 μm. Therefore, SPG pit parameters were reported with the left and right eye results averaged. On the other hand, the differences between the horizontal and vertical profiles were highly significant ($p < 0.0005$) for all goodness of fit measures and pit parameters. Therefore, horizontal and vertical data were reported separately. Consequently, 1162 horizontal and 1162 vertical fovea-based measures were analysed.

Descriptive statistics were summarised and reported as means (S.D.s). The RMSE was used to assess and compare goodness of fit of the SPG and other models. Pit parameters between horizontal and vertical directions or among nasal, temporal, superior and inferior locations were compared to characterise SPG-defined foveal pit shape.

The intra-session repeatability of the SPG model pit parameters obtained from fitting three repeated scans of the same eye was quantified by calculating the intra-session standard deviation (square root of the mean repeated measure variances)[57] for each pit parameter. The intra-session standard deviation were presented both as the absolute value and as the percentage of the mean parameter value. Intra-class correlation coefficients were used to assess repeatability of the SPG pit bottom width measures.

The Bayesian Information Criteria (BIC) was used to select the most appropriate model for the data. The BIC is the weighted difference of model complexity and goodness of fit so that models with more than necessary coefficients (overfitting) are penalised. When the same set of data is fitted by several models, the model with the smallest BIC value is considered to have the best combination of model complexity and goodness of fit and thus is preferred. The unpreferred models may have poorer goodness of fit, too many coefficients or both, compared to the preferred model.[58] Because BIC comparison is valid only when applied to the same set of data, only the seven model fits to the narrow dataset, Gaussian, sloped Gaussian, SPG, DoG_{NR}, DoG_{NR}, $oDoG_{NR}$ and $oDoG_{NR}$, were compared. To analyse model preference, BIC values of all tested models were computed for the same profile. BICs from intra-eye repeated scans were averaged. The model that produced the smallest BIC was designated as the preferred model for that fovea. This resulted in a percentage model preference distribution for all seven models. Because the SPG model differed from all comparison models by having a dedicated coefficient for flat bottoms, the analysis was repeated at different cut-offs of bottom flatness, λ. For $\lambda \geq 0$ μm, all 2324 (1162 horizontal and 1162 vertical) profiles were analysed, for $\lambda \geq 20$ μm, 1298 profiles were analysed, for $\lambda > 40$ μm, 1009 profiles and so on, as shown in Figure 9.

Results

SPG model

Goodness of fit—Overall, the SPG fitted the foveal pit data very well. Figure 4 shows the best-fitting SPG curves for data from four example vertical profiles representing different foveal asymmetries and bottom flatness. The yellow circles were landmarks generated by the SPG. The distributions of RMSE values of the 1162 horizontal and 1162 vertical profiles are presented in Figure 5. The mean RMSEs for the horizontal and vertical foveal profiles are 4.25 μm (95% CI: 4.20 and 4.30) and 3.89 (95% CI: 3.86 and 3.93), respectively. To provide a reference to goodness of the fits, we considered the inherited error in fitting quantised data. The mean squared error of quantising a continuous variable to integer pixels is $\Delta = (1)^2/12 = 0.0833$.[59] The RMSE is $\sqrt{\Delta} = 0.289$ pixels. Because each A-line step is 3 μm, even a perfect fit of quantized data should have an RMSE of $3^*\sqrt{\Delta} = 0.866$ μm.

Characterisation of foveal pit—Table 1 presents the mean pit parameters obtained from the SPG model fit. Results are shown for All Profiles and for pit bottom width classified as either Round Bottom Profiles ($\lambda \leq 30$ μm) or Flat Bottom Profiles ($\lambda > 30$ μm), determined by the SPG fitting. As shown in Figure 6, the SPG revealed a wide range of pit bottom widths. To facilitate understanding of the effect of bottom width, the bottom widths distribution was divided into these two categories, round bottom ($\lambda \leq 30$ μm) and flat bottom ($\lambda > 30$ μm). The 30 μm cut-off was selected because from this λ value onward, the SPG became the most preferred model over the other models (see Model Comparison section). All group comparisons (e.g., horizontal vs vertical minimum thickness, maximum thickness, etc.) presented in Table 1 were statistically significant at $p < 0.0005$, unless a p-value is given.

Overall characterisation—Overall, the foveal pits had the shape of a horizontal oval at the top and middle sections. The horizontal top and middle widths were significantly wider than that of vertical (top: 2120 (374) vs 1979 (318) μm, middle: 748 (159) vs 699 (138) μm). The wall heights, ordered by location from the highest to the lowest were superior (116 (22) μm), nasal (112 (21) μm), inferior (109 (21) μm) and temporal (95 (21) μm). The wall slopes, ordered by location from the steepest to the shallowest were superior (12.92 (2.68)°), inferior (12.51 (2.53)°), nasal (11.15 (2.52)°) and temporal (10.19 (2.55)°). The pit was shallower in horizontal profiles than in vertical profiles (104 (20) μm vs 113 (21) μm). The overall pit depth was 108 (20) μm. The maximum retinal thicknesses around the pit, ordered by location from the thickest to the thinnest, were superior (324 (17) μm), nasal (319 (17) μm), inferior (316 (16) μm) and temporal (301 (17) μm). The overall minimum thickness was 207 (17) μm.

Pit bottom shape—Figure 6 shows the histogram of the pit bottom width or the coefficient λ determined by the SPG fit. Overall, 714 (444 horizontal and 270 vertical) foveal profiles (30.7% out of the total 2324 profiles) were best fitted with a round bottom ($\lambda = 0$). The remaining pit bottoms formed a continuum of flat bottom widths, 49.1% of all foveal profiles with a bottom width $\lambda > 30$ μm, 23.1% with $\lambda > 100$ μm, 7.2% with $\lambda > 200$ μm, and 2.6% with $\lambda > 300$ μm. The shape of the pit bottom is less consistent than the

pit top, with 26.8% of the 1162 fovea pits being wider in the horizontal direction, 56.0% wider in the vertical direction and 17.2% having equal bottom widths in the two directions (including $\lambda = 0$ in both directions). An example of a profile with a very wide flat bottom by the SPG model fit is shown in the inset of Figure 6. This subject had six scans from both eyes (three scans/eye). The bottom widths of the six horizontal and six vertical profiles of the two eyes of the same subject ranged from 374 to 620 μm and from 149 to 501 μm, respectively. The range in these pit bottom width measures might reflect variances among the intra-eye repeated scans, between the two eyes of the same subject, between different directions and segmentation errors. The pit bottom widths of the two eyes estimated by the SPG model are highly correlated ($r = 0.73$) as shown in the scatter plot of Figure 7.

Foveal pits with flat bottoms ($\lambda > 30$ μm) had significantly different shapes from those with round bottoms ($\lambda \leq 30$ μm) in most pit measures (Table 1). Pits with flat bottoms tended to be deeper, wider at the top and in the middle, and had higher, steeper walls than pits with round bottoms. These comparisons suggest that foveal pits with round and flat bottoms may have genuinely different structures.

Repeatability of foveal pit characterisation—The repeatability of the SPG model foveal pit fits was evaluated using the 1140 (97.9%) of the scan eyes that had three good quality scans taken in one session, typically within 1 min. The repeatability of each SPG-determined foveal pit parameter estimate was quantified by intra-session standard deviation (μm) and is shown as the absolute values and percentages of the mean parameter values in Table 2. Overall, all parameters showed good repeatability, with all of the variances falling within 9% of the mean parameter values. The maximum and minimum retinal thickness parameters had the best repeatability, i.e., lowest percentage intra-session standard deviations (1.9% and 2.7% of the mean thicknesses). Pit depth and pit width parameters were less repeatable, with the intra-session standard deviations being 6% of the mean measures. Pit wall slopes showed the worst repeatability, with the intra-session standard deviation magnitude ~1.2°, which was 8.26% of the mean slope.

Foveal pit bottom width repeatability was evaluated using intra-class correlation coefficients. A high degree of repeatability was found among the three repeated measures of the pit bottom width of the same eye with a mean intra-class correlation coefficient of 0.86 (95% CI: 0.85–0.87; $p < 0.0005$).

SPG model summary—The SPG explicitly modelled the known variations of foveal pit shape, produced excellent goodness of fit, produced repeatable foveal pit characterisation, revealed systematic nasal/temporal and superior/inferior asymmetries in pit wall heights and slopes and demonstrated for the first time the existence of a continuum of pit bottom flatness.

Model comparisons

Goodness of fit—Figure 8 shows RMSE box plots for the SPG and the comparison models with varied coefficient restrictions and dataset widths. Horizontal (black boxes) and vertical (red boxes) profiles from both eyes were plotted separately. Numbers above the boxes are mean RMSE values for fitting all pits ($N = 1162$). Numbers below the boxes were

mean RMSEs from fitting pits with flat bottoms ($\lambda > 30$ μm; $N = 1141$; 485 horizontal and 656 vertical). All between model pair-wise comparisons showed highly significant differences ($p < 0.0005$), except between DoG_{WR} and DoG_{WU} ($p = 1.0$). Three trends were observed. Fitting the narrow datasets (subscript *N*) produced smaller RSMEs than fitting the wide datasets (subscript *W*), indicating that excluding parafoveal data improved model fitting. The asymmetric models (oDoG and SG) produced smaller RMSEs than their symmetric counterparts (DoG and G). Adding the flexibility in a model to fit flat bottoms (SPG) resulted in smaller RMSEs than SG, its round bottom counterpart. Therefore, the three key features that inspired the SPG model improved model goodness of fit in an additive manner. The $oDoG_{NU}$ fit was slightly but significantly better than the SPG fit, but this better performance was achieved from the $oDoG_{NU}$ model overfitting the data, as shown in the Model Fidelity section below.

Model complexity (number of model coefficients and goodness of fit)— Increasing the number of model coefficients usually leads to better goodness of fit, but too many coefficients (overfitting) can result in unintended outcomes. The Bayesian information criterion is a quantitative measure of the relative appropriateness among models of different complexities (i.e., number of coefficients). Figure 9 shows model preference at different pit bottom width cut-offs. When all pits were considered ($\lambda \geq 0$), the $oDoG_{NU}$ model was preferred (had the smallest BIC values) in 58.2% of the foveal profiles, compared to the SPG's 25.8%. However, when analyses were focused more on pits with flat bottoms (i.e., increasing λ cut-offs), the SPG became the most preferred model. For pits with bottoms wider than 30 μm, the SPG was clearly the most preferred model.

Model fidelity—The SPG model always produced the prototype pit curves that had smooth sigmoidal walls (dashed green curves in Figure 10), but such curves sometimes failed to follow the local variation of the data, thus compromising goodness of fit. On the other hand, the DoG or oDoG models could follow the data more closely, producing better goodness of fit, but also producing curves that deviated from their prototype pit. For example, the red $oDoG_{NU}$ curves in Figure 10 had a bent or a bump on one pit wall or a bump at the pit bottom. Such distortions could lead to an erroneous pit characterisation. A bent on a wall (Figure 10a) or a bump at the bottom (Figure 10c) would produce more local peaks or zero-crossings in the first derivative curve than specified by the oDoG or DoG landmark extract methods. Using a program that counted the number of zero-crossings, peaks and troughs in the first derivative of each best-fitting curve, we found that 32.6% of curves produced by the $oDoG_{NU}$ fit had one distorted wall. To test the consistency of the occurrence of the bent walls, we classified model curves as having no bent wall (0), a bent left wall (1) or a bent right wall (2). Among the 1140 eyes that had three good scans, 490 (43%) had three best fitting curves that had no distorted walls, 39 (3.4%) had three bent left walls and 29 (2.5%) had three bent right walls. The rest 582 (51%) eyes had various mixtures of no bent walls, bent left walls and bent right walls. Had bent walls been 'real' features of the foveal pit, they should have occurred more consistently on the same side of the same pit. In addition, 24 $oDoG_{NU}$ curves had a bump at the bottom. In contrast, when oDoG coefficient space was restricted ($oDoG_{NR}$), no distortions were detected. Therefore, the unrestricted oDoG model

may have too much freedom to follow local data variations that might not be real foveal pit features.

Because the distorted $oDoG_{NU}$ fits could fit small undulation in the data more closely, they might have given the $oDoG_{NU}$ an edge over SPG in goodness of fit. Indeed, the mean RMSE of the distorted $oDoG_{NU}$ curves was 3.837 (0.884) μm vs corresponding SPG curves' 3.983 (0.895) μm. Restricting the coefficient space of the oDoG model to $d > 1$, $e < 1$ and $-17 < \Delta\mu < 17$ ($oDoG_{NR}$ fit) eliminated distortions in the fitting curves, but it also reduced their goodness of fit. The RMSE of the $oDoG_{NR}$ fit, 4.44 (1.247) μm, was significantly inferior to those of the SPG fit.

These results demonstrate that a comprehensive model evaluation should include goodness of fit, model complexity and model fidelity. Using these criteria, the SPG was the best model overall among the models tested.

Discussion

In this study we developed a new mathematical model, the sloped piecemeal Gaussian (SPG) model, to characterise the shape of the foveal pit. When applied to the OCT data from pairs of foveas of 581 young adult subjects, the SPG provided excellent fits to pits with a wide range of asymmetries and bottom widths and produced highly repeatable pit characterisation, extending the capabilities of previous models. Using the SPG model, we demonstrated consistent asymmetry in foveal pit wall heights and slopes in both horizontal and vertical directions and revealed a continuum of flat pit bottoms in humans. A comparison of the SPG with several existing models showed that the three key features of the SPG model, focusing on data between the pit rims, allowing asymmetry in pit shape and introducing the flexibility for different pit bottom flatness, had additive effects on improving the model goodness of fit. Among the foveal pits best fitted with a flat bottom, the SPG was the most preferred model because it best combined high goodness of fit and appropriate model complexity. In addition, the SPG showed good model fidelity by producing the best distortion-free pit shape representations among the models tested. It is of note that while the SPG model was tested on OCT scans of human retinas in this study, it is a generic mathematical model inspired by extensive anatomic studies of human and animal retinas. Its application can be extended to foveal profiles from any imaging modalities (e.g. MRI, ultrasonography, anatomy) and other species (e.g. simians).[3,49,60]

SPG features

Flat pit bottom—The most important contribution of the SPG is its ability to show the existence of a continuum of pit bottom widths, ranging from round bottoms to flat bottoms as wide as 562 μm. Some early studies of human foveal morphology described pit bottoms as flat[61,62] but others reported them as round.[60,63] Polyak speculated that there might be a wide individual variation in pit bottom shapes.[60] With the SPG model, we confirmed Polyak's speculation.

A major advantage of introducing a flat pit bottom to the SPG model is the ability to fit pit width and wall slope independently. In a Gaussian model (Equation 1), for example, the mid

width of the pit is proportional to σ and the maximum slope is proportional to $1/\sigma^2$. Therefore, the same coefficient σ defines both pit width and wall slope. In comparison, the wall slope of a SPG model is still proportional to $1/\sigma^2$, but it mid-width is now proportional to $\sigma + \lambda$. The flat bottom coefficient λ provides an independent manipulation of the pit width without changing the wall slope. Consequently, the SPG model can provide a close fit and accurate characterisation to wide pits with shallow walls and round bottoms (bowl shaped) as well as wide pits with steep walls and flat bottoms (pan shaped). The dissociation of pit width and wall slope in the SPG model predicts a lower correlation between these parameters than would be predicted by other models. Indeed, the correlation between the pit mid-width and wall slope obtained by the flat-bottomed SPG model, $r = 0.44$, was lower than that obtained by the round-bottomed sloped Gaussian model, $r = 0.58$. Furthermore, a comparison of the pit parameters determined by the round-bottom sloped Gaussian model and the flat-bottom SPG model showed that when all pits were considered, the walls of SPG fits were 0.50 (0.72)° steeper and the minimum retinal thicknesses were 2.1 (2.6) μm thicker than those of the round-bottom sloped Gaussian fits. When limiting the comparison to pits with more pronounced flat bottoms ($\lambda > 30$ μm), the SPG walls were 0.96 (0.79)° steeper and its minimum retinal thickness was 4.0 (2.54) μm thicker than those of the sloped Gaussian fits. Because the SPG model had better goodness of fit than the sloped Gaussian model, the SPG parameters represent more accurate characterisation of the foveal pits. It is of note that the magnitude of the improvement brought about by introducing a flat bottom into the model, i.e., 2–4 μm in minimum thickness and 0.5–1° in wall slope, is in the same magnitude as the previously reported differences among sex, race, age and amblyopic sub-populations,[18,44,46] suggesting that the SPG can become a more powerful tool for clinicians and researchers to differentiate normal variations and to quantify the impacts of diseases on the foveal pit.

Asymmetry—While the nasal/temporal asymmetry is a known anatomical feature of the foveal pit,[60,62] to our knowledge, this study is the first systematic analysis of foveal pit asymmetry on a large sample of young adult OCT macular scans. Using the SPG model, we not only quantified the known nasal/temporal asymmetry but also provided strong evidence for the existence of superior/inferior asymmetry. In both horizontal and vertical directions, both the wall height and wall slope were asymmetric.

Location of rims—The SPG model limited fitting to the narrow dataset and produced much better goodness of fit than the DoG or oDoG models fitting the wide dataset (Figure 8). However, without fitting the parafoveal data, the SPG determined the rim point landmarks $\mathscr{R}$ and $\mathscr{R}$' by finding the locations where the curve deviated from the asymptotic line by a preset amount (Figure 3). This is different from the DoG and oDoG models that fit the parafoveal data and explicitly determine $\mathscr{R}$ and $\mathscr{R}$' as the local maximums.[43,44] This difference raises questions about the accuracy of SPG landmark placement and the resultant pit top widths and maximum thickness values. To address this concern, an analysis was performed to compare the SPG rim points with model-free rim points obtained by the local peaks of the smoothed raw data. On average, the SPG-determined pit top width was 13.7 pixels (102 μm) or 4.65% narrower than that determined by the smoothed raw data peaks. In contrast, the oDoG_{WR}, which fitted the parafoveal data and determined the rim points

explicitly, produced a mean top width that was 16.0 pixels (120 μm) or 5.55% narrower than that determined by raw data peaks. Therefore, the SPG rim points and their derived pit parameters were at least comparable to (or better than) those determined by an oDoG model that explicitly fits the rim points.

Data-driven vs model-driven approaches—One of the major differences between the model-driven and data-driven approaches is the role of prior knowledge about the shape to be modelled. Our modelling effort was based on the knowledge accumulated from many anatomic studies of human and simian retinas,[60-63] which all illustrated the fovea as an indentation in the retina that had smooth, sigmoidal walls and a round or flat bottom. The SPG was a function specifically developed to realise this knowledge. The model coefficients had explicitly defined relationship with pit parameters. In comparison, the data-driven approach does not require any prior knowledge to fit the OCT data. The same spline or symbolic regression methods can be used to fit any shape. The coefficients of best-fitting curve may not be directly related to the pit shape.

The data-driven curve fitting has also been successfully used to characterise foveal shape. Knighton *et al*.[40] used a two-dimensional penalised spline method to generate representations of the shapes of the Ganglion Cell + Inner Plexiform layers of human macula. The foveal wall was represented by the sum of a set of small, overlapping basis functions with best-fitting weights. The pit parameters were then derived from the spline. For example, the wall slope was determined by a linear regression through a segment of the wall. Symbolic regression is another data-driven method, in which mathematical operators, such as plus, minus, multiplication, division, power, sine and cosine, are freely combined to form equations. The equation that produced the smallest error from the OCT data was the representation of the pit. Using this method, it was found that increasing complexity of the best-fitting equation (larger number of operators in the equation) correlated with increasing age of normal subjects[42] and with increasing risk of macular hole formation.[41]

Limitations—The SPG was built on the knowledge obtain from foveal pit without significant ocular pathology. Therefore, its application to foveas undergoing gross pathological changes, such as in advanced macular degeneration or diabetic retinopathy, may be limited. This is because building a good model requires prior knowledge about the manifestation the underlying pathology, such as the number, location and extent of drusen or neovascularisation, but such knowledge may not be readily available. Therefore, data-driven curve fitting, because of its ability to follow random shape variations, may be better suited in quantifying grossly deformed foveas.

While representing the flat pit bottoms with a line segment works well with current OCT scans, it cannot capture some of the subtler details known to human foveas, for example, a 5 to 6-cone wide depression at the centre of a flat foveal floor (Schwalbe 1887, cited by Polyak[60]). Models for future high-resolution OCT or anatomic images may need to incorporate this feature, for example, by adding a second, very small Gaussian model on the floor of the fovea. Similarly, if future imaging and anatomical studies provide clear evidence that human foveal walls are not sigmoid but bent, the SPG model can be modified to incorporate this new knowledge.

The SPG is a piecemeal continuous function, which may miss a very sharp change of the curve, such as the sharp corner in the insert of Figure 6. Such an error, though small and unlikely to inflate the RMSE, may nevertheless affect pit characterisation, for example, underestimating the width of the pit bottom. The SPG is a two-dimensional function, fitting one profile a time. Its ability to quantify 3D foveal pit measures, such as the pit volume, has yet to be tested. There are data-driven methods, such as 2D penalised Splines, that may be more apt to fit 3D surfaces.[40]

The SPG model was designed to fit the foveal pit and cannot be extended beyond the rim points. If the need ever arises for fitting the fovea beyond the rim, for example, in dome-shaped macula associated with high myopia (−6 dioptres or more),[64-66] more complex models, for example, a sloped piecemeal DoG model, may need to be constructed and tested.

We only compared the SPG with 10 variations of Gaussian-based and DoG-based fits. There may be other models that compete more favourably with the SPG in goodness of fit. However, the comparison between the SPG and $oDoG_{NU}$ fits suggests that the room for goodness of fit improvement has become small. A newer, better model needs strong evidence to incorporate new foveal features.

Conclusions

Using foveal scans from a large sample of young adult myopes and non-myopes, the Sloped Piecemeal Gaussian was shown to be a parsimonious mathematical model that provides excellent fit and faithful characterisation of foveal pit shape and its known variations. This new model should be easily adopted for automated online or offline analysis of foveal pit data from OCT and other imaging modalities. A recent COMET analysis of the Early Treatment Diabetic Retinopathy Study macular thickness maps has shown that central and parafoveal retinal thickness varies by sex, ethnicity and refractive error in myopes and non-myopes,[31] suggesting variations in foveal shapes. The more accurate, model-based characterisation achieved by fitting foveal shape profiles with the SPG model is likely to achieve more robust and more informative classification of these groups.

Acknowledgements

This study was supported by the following National Eye Institute (United States) grants: EY11805, EY11740, EY11756, EY11754, EY11752, EY11755.

References

1. Wall GL. Significance of the foveal depression. Arch Ophthalmol 1937; 18: 912–919.
2. Pumphrey RJ. The theory of the fovea. J Exp Biol 1948; 25: 299–312.
3. Harkness L & Bennet-Clark HC. The deep fovea as a focus indicator. Nature 1978; 272: 814–816. [PubMed: 643070]
4. Williams DR. Visual consequences of the foveal pit. Invest Ophthalmol Vis Sci 1980; 19: 653–667. [PubMed: 7380624]
5. Locket NA. Problems of deep foveas. Aust N Z J Ophthalmol 1992; 20: 281–295. [PubMed: 1295523]
6. Hendrickson AE & Yuodelis C. The morphological development of the human fovea. Ophthalmology 1984; 91: 603–612. [PubMed: 6462623]

7. Yuodelis C & Hendrickson A. A qualitative and quantitative analysis of the human fovea during development. Vision Res 1986; 26: 847–855. [PubMed: 3750868]
8. Springer AD & Hendrickson AE. Development of the primate area of high acuity. 2. Quantitative morphological changes associated with retinal and pars plana growth. Vis Neurosci 2004; 21: 775–790. [PubMed: 15683563]
9. Springer AD & Hendrickson AE. Development of the primate area of high acuity. 1. Use of finite element analysis models to identify mechanical variables affecting pit formation. Vis Neurosci 2004; 21: 53–62. [PubMed: 15137581]
10. Springer AD & Hendrickson AE. Development of the primate area of high acuity, 3: temporal relationships between pit formation, retinal elongation and cone packing. Vis Neurosci 2005; 22: 171–185. [PubMed: 15935110]
11. Provis JM, Penfold PL, Cornish EE, Sandercoe TM & Madigan MC. Anatomy and development of the macula: specialisation and the vulnerability to macular degeneration. Clin Exp Optom 2005; 88: 269–281. [PubMed: 16255686]
12. Chan A, Duker JS, Ko TH, Fujimoto JG & Schuman JS. Normal macular thickness measurements in healthy eyes using Stratus optical coherence tomography. Arch Ophthalmol 2006; 124: 193–198. [PubMed: 16476888]
13. Asefzadeh B, Cavallerano AA & Fisch BM. Racial differences in macular thickness in healthy eyes. Optom Vis Sci 2007; 84: 941–945. [PubMed: 18049358]
14. Kelty PJ, Payne JF, Trivedi RH, Kelty J, Bowie EM & Burger BM. Macular thickness assessment in healthy eyes based on ethnicity using Stratus OCT optical coherence tomography. Invest Ophthalmol Vis Sci 2008; 49: 2668–2672. [PubMed: 18515595]
15. Grover S, Murthy RK, Brar VS & Chalam KV. Normative data for macular thickness by high-definition spectral-domain optical coherence tomography (spectralis). Am J Ophthalmol 2009; 148: 266–271. [PubMed: 19427616]
16. Ooto S, Hangai M, Sakamoto A et al. Three-dimensional profile of macular retinal thickness in normal Japanese eyes. Invest Ophthalmol Vis Sci 2010; 51: 465–473. [PubMed: 19696169]
17. Song WK, Lee SC, Lee ES, Kim CY & Kim SS. Macular thickness variations with sex, age, and axial length in healthy subjects: a spectral domain-optical coherence tomography study. Invest Ophthalmol Vis Sci 2010; 51: 3913–3918. [PubMed: 20357206]
18. Kashani AH, Zimmer-Galler IE, Shah SM et al. Retinal thickness analysis by race, gender, and age using Stratus OCT. Am J Ophthalmol 2010; 149: 496–502 e491. [PubMed: 20042179]
19. Duan XR, Liang YB, Friedman DS et al. Normal macular thickness measurements using optical coherence tomography in healthy eyes of adult Chinese persons: the Handan Eye Study. Ophthalmology 2010; 117: 1585–1594. [PubMed: 20472290]
20. Tariq YM, Li H, Burlutsky G & Mitchell P. Ethnic differences in macular thickness. Clin Experiment Ophthalmol 2011; 39: 893–898. [PubMed: 21575119]
21. Tick S, Rossant F, Ghorbel I et al. Foveal shape and structure in a normal population. Invest Ophthalmol Vis Sci 2011; 52: 5105–5110. [PubMed: 21803966]
22. Adhi M, Aziz S, Muhammad K & Adhi MI. Macular thickness by age and gender in healthy eyes using spectral domain optical coherence tomography. PLoS One 2012; 7: e37638. [PubMed: 22629435]
23. Li T, Zhou X, Wang Z, Zhu J, Shen W & Jiang B. Assessment of retinal and choroidal measurements in Chinese school-age children with cirrus-hd optical coherence tomography. PLoS One 2016; 11: e0158948. [PubMed: 27391015]
24. Patel PJ, Foster PJ, Grossi CM et al. Spectral-domain optical coherence tomography imaging in 67 321 adults: associations with macular thickness in the UK Biobank Study. Ophthalmology 2016; 123: 829–840. [PubMed: 26746598]
25. Morgan IG, Ohno-Matsui K & Saw SM. Myopia. Lancet 2012; 379: 1739–1748. [PubMed: 22559900]
26. Liu HH, Xu L, Wang YX, Wang S, You QS & Jonas JB. Prevalence and progression of myopic retinopathy in Chinese adults: the Beijing Eye Study. Ophthalmology 2010; 117: 1763–1768. [PubMed: 20447693]

27. Lim MC, Hoh ST, Foster PJ et al. Use of optical coherence tomography to assess variations in macular retinal thickness in myopia. Invest Ophthalmol Vis Sci 2005; 46: 974–978. [PubMed: 15728555]
28. Wu PC, Chen YJ, Chen CH et al. Assessment of macular retinal thickness and volume in normal eyes and highly myopic eyes with third-generation optical coherence tomography. Eye (Lond) 2008; 22: 551–555. [PubMed: 17464309]
29. Xie R, Zhou XT, Lu F et al. Correlation between myopia and major biometric parameters of the eye: a retrospective clinical study. Optom Vis Sci 2009; 86: E503–E508. [PubMed: 19349927]
30. Zhang Z, He X, Zhu J, Jiang K, Zheng W & Ke B. Macular measurements using optical coherence tomography in healthy Chinese school age children. Invest Ophthalmol Vis Sci 2011; 52: 6377–6383. [PubMed: 21743016]
31. Harb E, Hyman L, Fazzari M, Gwiazda J, Marsh-Tootle W & Group CS. Factors associated with macular thickness in the COMET myopic cohort. Optom Vis Sci 2012; 89: 620–631. [PubMed: 22525127]
32. Hwang YH & Kim YY. Macular thickness and volume of myopic eyes measured using spectral-domain optical coherence tomography. Clin Exp Optom 2012; 95: 492–498. [PubMed: 22759271]
33. Lim HT & Chun BY. Comparison of OCT measurements between high myopic and low myopic children. Optom Vis Sci 2013; 90: 1473–1478. [PubMed: 24121408]
34. Chen S, Wang B, Dong N, Ren X, Zhang T & Xiao L. Macular measurements using spectral-domain optical coherence tomography in Chinese myopic children. Invest Ophthalmol Vis Sci 2014; 55: 7410–7416. [PubMed: 25316719]
35. Song AP, Wu XY, Wang JR, Liu W, Sun Y & Yu T. Measurement of retinal thickness in macular region of high myopic eyes using spectral domain OCT. Int J Ophthalmol 2014; 7: 122–127. [PubMed: 24634877]
36. Ziylan S, Kiziloglu OY, Yenerel NM, Gokce B & Ciftci F. Macular thickness in highly myopic children aged 3 to 7 years. J Pediatr Ophthalmol Strabismus 2015; 52: 282–286. [PubMed: 26046482]
37. Zhao MH, Wu Q, Hu P & Jia LL. Macular thickness in myopia: an OCT study of young Chinese patients. Curr Eye Res 2016; [Epub ahead of print]. http://www.tandfonline.com/doi/full/10.3109/02713683.2015.1119854.
38. Samuel NE & Krishnagopal S. Foveal and macular thickness evaluation by spectral OCT SLO and its relation with axial length in various degree of myopia. J Clin Diagn Res 2015; 9: NC01–NC04.
39. Hung KC, Wu PC, Poon YC et al. Macular diagnostic ability in OCT for assessing glaucoma in high myopia. Optom Vis Sci 2016; 93: 126–135. [PubMed: 26704143]
40. Knighton RW & Gregori G. The shape of the ganglion cell plus inner plexiform layers of the normal human macula. Invest Ophthalmol Vis Sci 2012; 53: 7412–7420. [PubMed: 23033389]
41. Barak Y, Sherman MP & Schaal S. Mathematical analysis of specific anatomic foveal configurations predisposing to the formation of macular holes. Invest Ophthalmol Vis Sci 2011; 52: 8266–8270. [PubMed: 21911580]
42. Nesmith B, Gupta A, Strange T, Schaal Y & Schaal S. Mathematical analysis of the normal anatomy of the aging fovea. Invest Ophthalmol Vis Sci 2014; 55: 5962–5966. [PubMed: 25168895]
43. Dubis AM, McAllister JT & Carroll J. Reconstructing foveal pit morphology from optical coherence tomography imaging. Br J Ophthalmol 2009; 93: 1223–1227. [PubMed: 19474001]
44. Bruce A, Pacey IE, Bradbury JA, Scally AJ & Barrett BT. Bilateral changes in foveal structure in individuals with amblyopia. Ophthalmology 2013; 120: 395–403. [PubMed: 23031668]
45. Scheibe P, Lazareva A, Braumann UD et al. Parametric model for the 3D reconstruction of individual fovea shape from OCT data. Exp Eye Res 2014; 119: 19–26. [PubMed: 24291205]
46. Wagner-Schuman M, Dubis AM, Nordgren RN et al. Race- and sex-related differences in retinal thickness and foveal pit morphology. Invest Ophthalmol Vis Sci 2011; 52: 625–634. [PubMed: 20861480]
47. Chui TY, Zhong Z, Song H & Burns SA. Foveal avascular zone and its relationship to foveal pit shape. Optom Vis Sci 2012; 89: 602–610. [PubMed: 22426172]

48. Wilk MA, McAllister JT, Cooper RF et al. Relationship between foveal cone specialization and pit morphology in albinism. Invest Ophthalmol Vis Sci 2014; 55: 4186–4198. [PubMed: 24845642]
49. Moore BA, Yoo I, Tyrrell LP, Benes B & Fernandez-Juricic E. FOVEA: a new program to standardize the measurement of foveal pit morphology. PeerJ 2016; 4: e1785. [PubMed: 27076997]
50. Michaelides M, Rha J, Dees EW et al. Integrity of the cone photoreceptor mosaic in oligocone trichromacy. Invest Ophthalmol Vis Sci 2011; 52: 4757–4764. [PubMed: 21436275]
51. Ding Y, Spund B, Glazman S et al. Application of an OCT data-based mathematical model of the foveal pit in Parkinson disease. J Neural Transm 2014; 121: 1367–1376. [PubMed: 24748549]
52. Rock T, Wilhelm B, Bartz-Schmidt KU & Rock D. The influence of axial length on confocal scanning laser ophthalmoscopy and spectral-domain optical coherence tomography size measurements: a pilot study. Graefes Arch Clin Exp Ophthalmol 2014; 252: 589–593. [PubMed: 24562463]
53. Kuo AN, McNabb RP, Chiu SJ et al. Correction of ocular shape in retinal optical coherence tomography and effect on current clinical measures. Am J Ophthalmol 2013; 156: 304–311. [PubMed: 23659972]
54. Optovue. RTVue RT-100 User's Manual. Optovue, Inc: Fremont, CA, 2009.
55. Varma R & Sinai MJ. The normative database for the RTVue In: Glaucoma (Weinreb RN & Varma R, editors), Optovue: Fremont, CA, 2009; pp. 19–39.
56. Armstrong RA. Statistical guidelines for the analysis of data obtained from one or both eyes. Ophthalmic Physiol Opt 2013; 33: 7–14. [PubMed: 23252852]
57. Bland JM & Altman DG. Measurement error. BMJ 1996; 313: 744. [PubMed: 8819450]
58. Akaike H A new look at the statistical model identification. IEEE Trans Autom Control 1974; 19: 716–723.
59. Oliver BM, Pierce JR & Shanon CE. The Philosophy of PCM. Proc IRE 1948; 36: 1324–1331.
60. Polyak SL. The Retina. University of Chicago Press: Chicago, 1941.
61. Dimmer F Beitrage zur Anatomie und Physiologie der Macula Lutea des Menschen. Franz Deuticke: Leipzig, Germany, 1894.
62. Salzmann M The Anatomy and Histology of The Human Eyeball in the Normal State - Its Development and Senescence. The University of Chicago Press: Chicago, 1912.
63. Golding-Bird CH & Schafer EA. Observations on the structure of the central fovea of the human eye. Internationalen Monatsschrift f Anat u Phys 1895; XII: Available from: https://books.google.com/books?id=1m8sAQAAIAAJ&pg=RA3-PA3&lpg=RA3-PA3&dq=Observations+on+the+structure+of+the+central+fovea+of+the+human+eye&source=bl&ots=OCZwOgBeWZ&sig=it84LBY76c7YPK-69UYtSo-9XPQ&hl=en&sa=X&ved=0ahUKEwiK_6WJ0YDPAhWE8x4KHQUaDVcQ6AEIJDAB#v=onepage&q=Observations%20on%20the%20structure%20of%20the%20central%20fovea%20of%20the%20human%20eye&f=false.
64. Ellabban AA, Tsujikawa A, Matsumoto A et al. Three-dimensional tomographic features of dome-shaped macula by swept-source optical coherence tomography. Am J Ophthalmol 2013; 155: 320–328 e322. [PubMed: 23127750]
65. Gaucher D, Erginay A, Lecleire-Collet A et al. Dome-shaped macula in eyes with myopic posterior staphyloma. Am J Ophthalmol 2008; 145: 909–914. [PubMed: 18342827]
66. Ohsugi H, Ikuno Y, Oshima K, Yamauchi T & Tabuchi H. Morphologic characteristics of macular complications of a dome-shaped macula determined by swept-source optical coherence tomography. Am J Ophthalmol 2014; 158: 162–170 e161. [PubMed: 24631474]

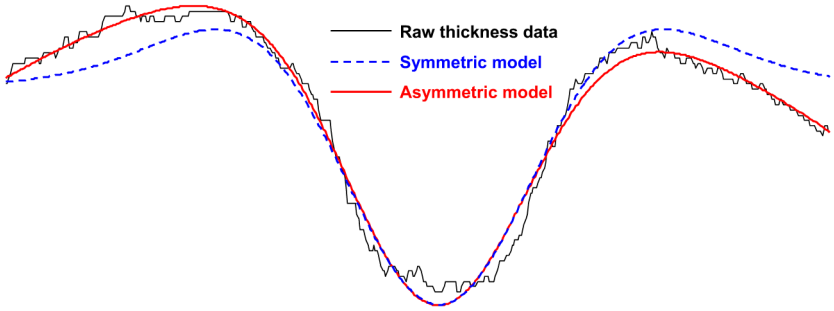

Figure 1.

Example of a misfit of a foveal pit with an extended flat bottom. The black curve represents the raw OCT retinal thickness data. The best fitting curves of a symmetric model (dashed blue curve) and an asymmetric model (solid red curve) do not fit this pit well.

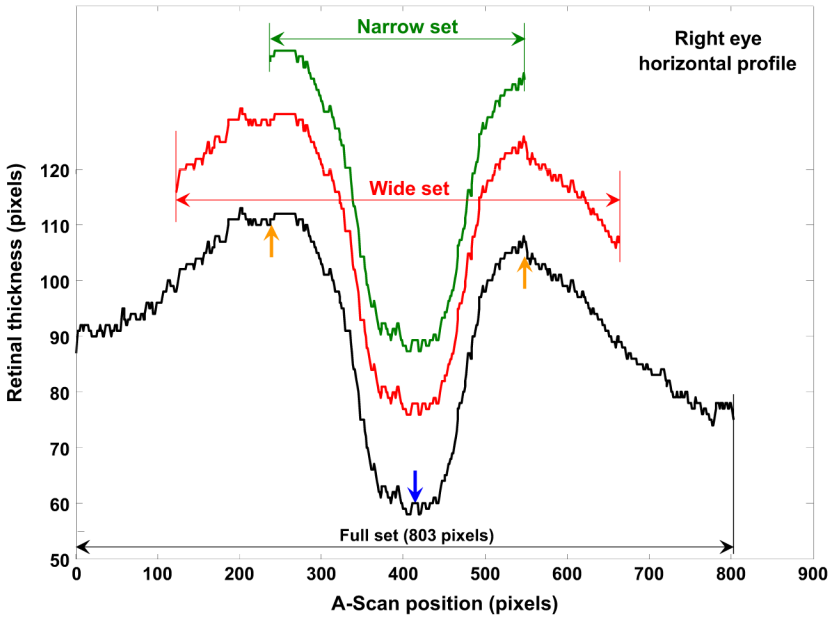

Figure 2.

Extents of data set. Black curve: full retinal thickness data set. Red curve: wide data set (including foveal and parafoveal data), used for Difference of Gaussian-based (DoG) and offset DoG (oDoG) model fits. Green curve: narrow data set (foveal data only), used for Gaussian-based, DoG-based and oDoG-based model fits. The blue arrow and orange arrows show the foveal pit centre and rims derived from the smoothed data of the foveal profile.

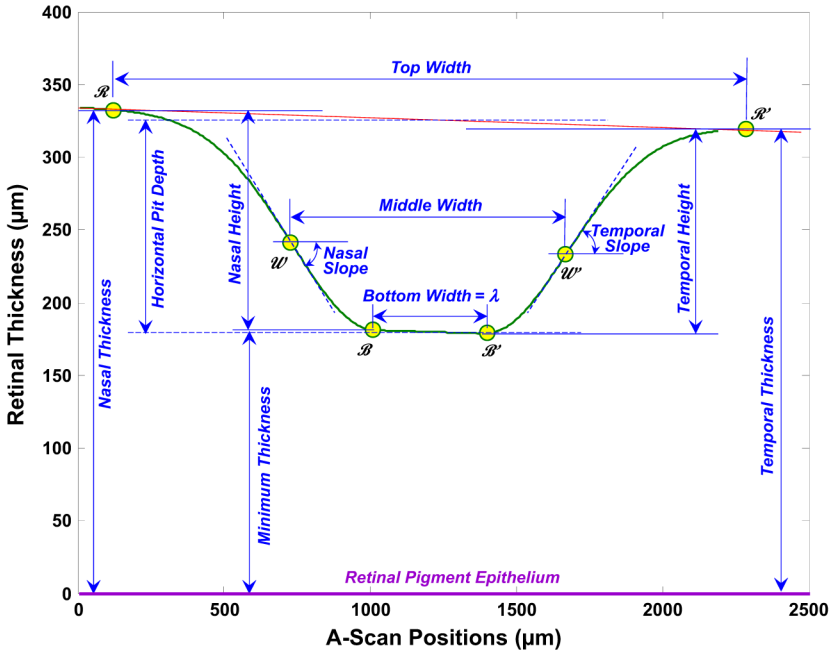

Figure 3.

Landmarks and pit parameters estimated from a Sloped Piecemeal Gaussian (SPG) fit of foveal pit data from a horizontal profile. The three sets of landmarks are represented by the yellow circles: Rim points, $\mathscr{R}$ and $\mathscr{R}$'; Wall points, $\mathscr{W}$ and $\mathscr{W}$'; and Bottom points, $\mathscr{B}$ and $\mathscr{B}$'. The green curve is a SPG model fitting curve. The red line is the asymptotic line of the SPG curve. The thick purple line is the Retinal Pigment Epithelium. Pit parameters are indicated in blue.

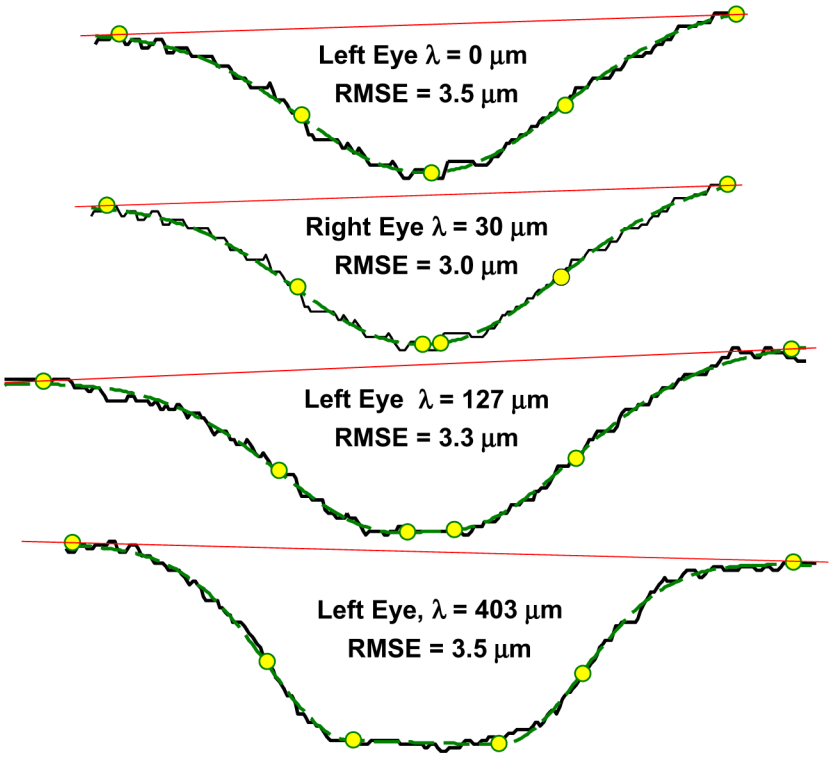

Figure 4.

Examples of sloped piecemeal Gaussian (SPG) fits to foveal pit data from four vertical profiles with different pit asymmetries and flat bottom widths. Black curves are the raw thickness data. Dashed green curves are the best fitting SPG functions. Yellow circles are the three sets of pit landmarks generated by the SPG fitting program. Red lines are the asymptotic lines of the SPG curves showing asymmetry. λ is SPG pit bottom width coefficient in μm; RMSE: Root Mean Square Error in μm.

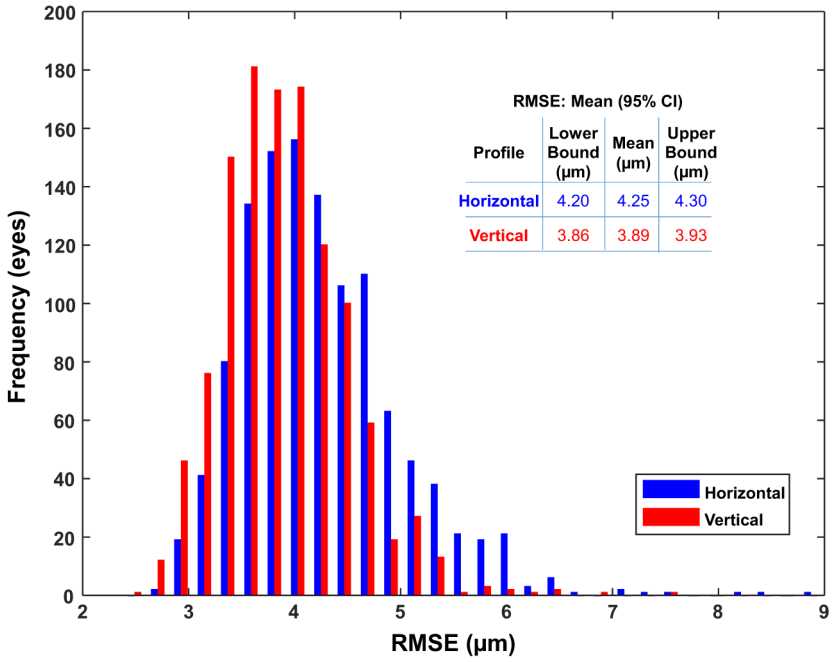

Figure 5.

Distributions of goodness of fit values for the Sloped Piecemeal Gaussian fits to 1162 horizontal (blue) and 1162 vertical (red) foveal profiles measured by Root Mean Square Error (RMSE).

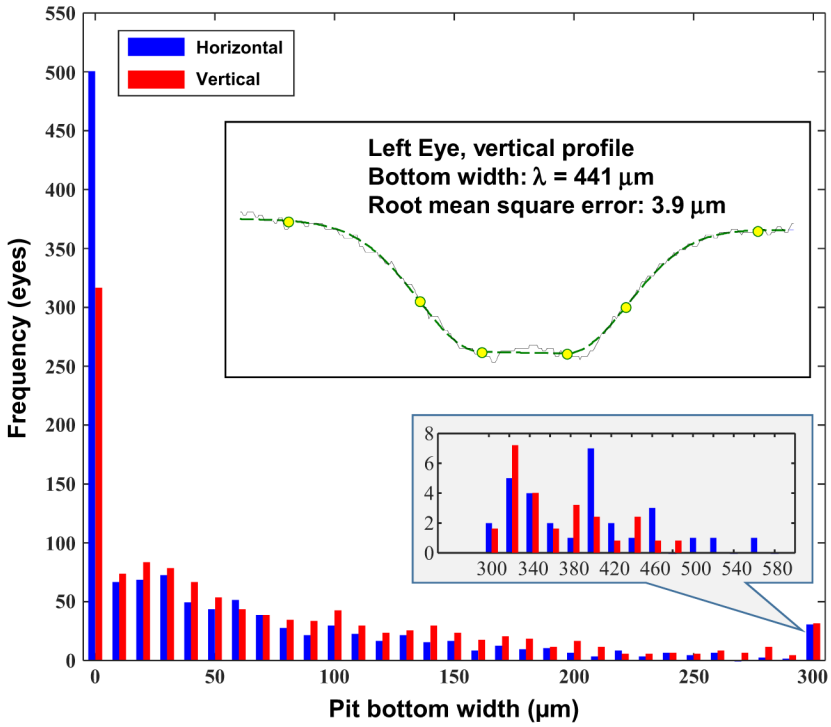

Figure 6.

Distributions of pit bottom widths determined by the Sloped Piecemeal Gaussian model fits of 1162 horizontal (blue bars) and 1162 vertical foveal profiles (red bars). The small histogram inset shows the details of the wider end of the pit bottom width spectrum. The inset in the top right hand corner shows an example of a SPG fit (green dashed curve) to a vertical profile with an extended flat bottom (black solid curve).

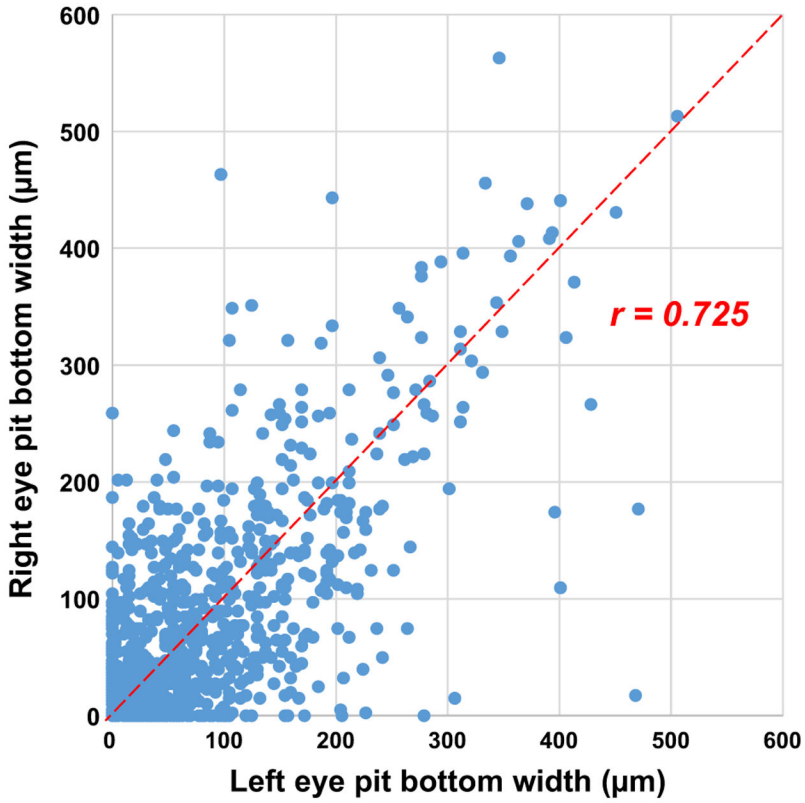

Figure 7.
Scatter plot of the left and right eye pit bottom widths determined by the Sloped Piecemeal Gaussian model (1162 pairs of horizontal and vertical profiles). The red dashed line is the 45 deg diagonal line.

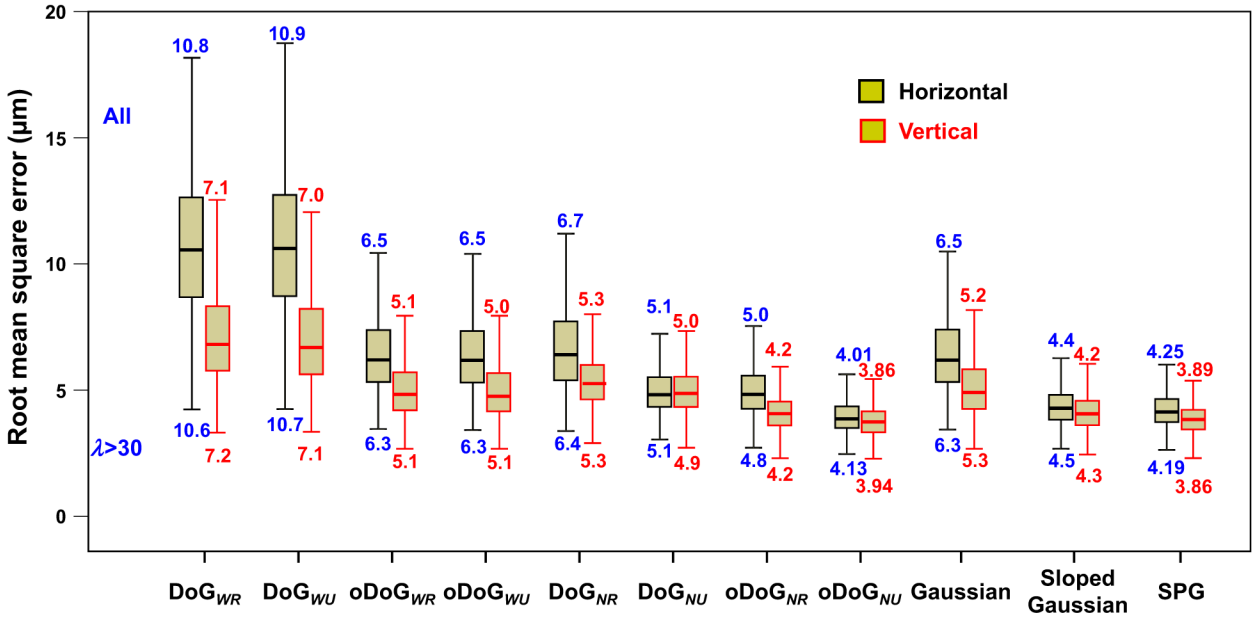

Figure 8.

Box plots of Root Mean Square Errors from different models fitting horizontal (black boxes) and vertical (red boxes) foveal profiles. *DoG$_{WR}$*: Restricted DoG model fitting wide dataset; *DoG$_{WU}$*: Unrestricted DoG model fitting wide dataset; oDoG$_{WR}$: Restricted offset DoG model fitting wide dataset; oDoG$_{WU}$: Unrestricted offset DoG model fitting wide dataset; *DoG$_{NR}$*: Restricted DoG model fitting narrow dataset; *DoGN$_{U}$*: Unrestricted DoG model fitting narrow dataset; oDoG$_{NR}$: Restricted offset DoG model fitting narrow dataset; oDoG$_{NU}$: Unrestricted offset DoG model fitting narrow dataset; *SPG*: sloped piecemeal Gaussian. Numbers above the boxes are mean RMSEs obtained from fitting all 1162 pits. Numbers below the boxes are mean RMSEs obtained from fitting 1141 pits with more pronounced bottom width ($\lambda > 30$ μm).

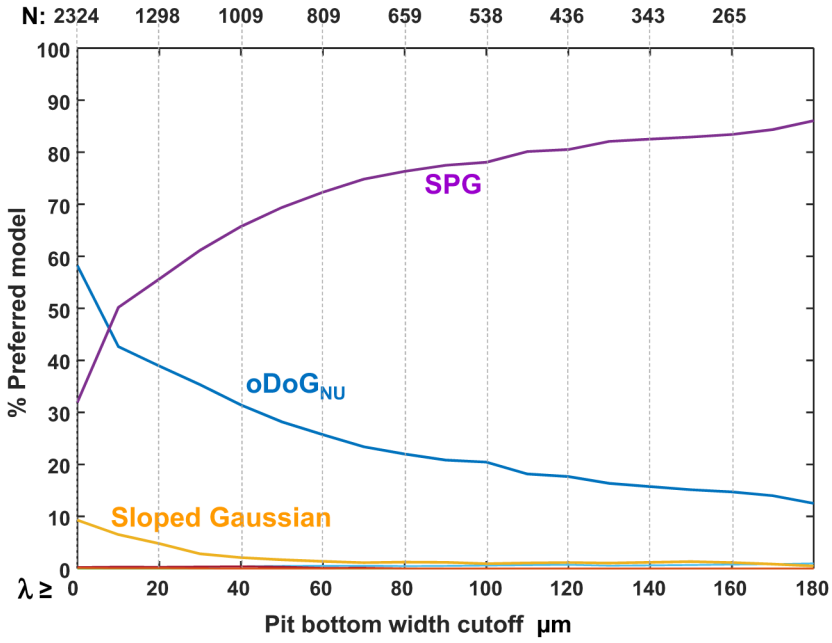

Figure 9.

Model preference. Percentages of pits that preferred the seven model fits are plotted at different pit bottom width cut-offs (λ ≥). The number of pits at each cut-off, *N*, is shown above the graph. Only the Sloped Gaussian model, Sloped Piecemeal Gaussian model (SPG) and unrestricted offset Difference of Gaussian model fitting the narrow dataset (oDoG$_{NU}$) were preferred by more than 1% of the pits at λ ≥ 0.

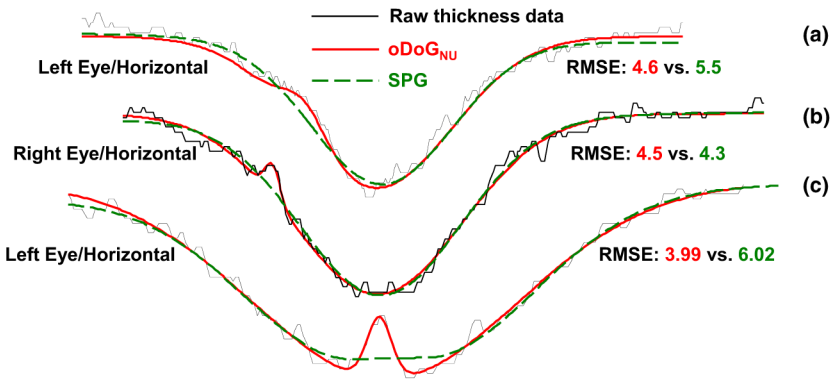

Figure 10.

Examples of poor model fidelity from fitting three horizontal profiles. Black curves are the raw thickness data. Solid red curves are unrestricted offset DoG fitting the narrow dataset (oDoG$_{NU}$). Dashed green curves are the sloped piecemeal Gaussian (SPG) fit. The oDoG$_{NU}$ fits follow local data variation more closely and have better goodness of fit (smaller RMSE) than the SPG fits, but the curves are distorted on the wall (a and b) or at the bottom (c). RMSE: Root Mean Square Error in μm.

Table 1.

Foveal pit parameters (mean (S.D.)) from Sloped Piecemeal Gaussian (SPG) model fits. The numbers are averages of the parameters from the two eyes of the subjects, presented separately for Horizontal and Vertical directions

		All		Round bottom		Flat bottom	
		Horizontal (*N* = 581)	Vertical (*N* = 581)	Horizontal (*N* = 339)	Vertical (*N* = 253)	Horizontal (*N* = 242)	Vertical (*N* = 328)
Pit parameters	**Location**	**Mean (S.D.)**	**Mean (S.D.)**	**Mean (S.D.)**	**Mean (S.D.)**	**Mean (S.D.)**	**Mean (S.D.)**
Thickness (μm)	Minimum	206 (17)	208 (17)	210 (16)	214 (17)	201 (16)	202 (15)
	Nasal/Superior	319 (17)	324 (17)	321 (16)	325 (16)	317 (16)	323 (17)
	Temporal/Inferior	301 (17)	316 (16)	303 (16)	318 (15)	298 (16)	315 (16)
	Maximum	310 (17)	320 (17)	312 (15)	321 (15)	308 (15)	319 (15)
Wall height (μm)	Nasal/Superior	112 (21)	116 (22)	110 (16)	111 (21)	115 (20)	120 (20)
	Temporal/Inferior	95 (21)	109 (21)	93 (20)	103 (21)	98 (20)	113 (19)
Pit depth (μm)	Mean Depth	104 (20)	113 (21)	102 (20)	108 (21)	107 (20)	117 (20)
Width (μm)	Top	2120 (374)	1979 (318)	2064 (335)	1913 (293)	2197 (369)	2028 (299)
	Mid	748 (159)	699 (138)	700 (127)	638 (106)	816 (162)	745 (133)
Wall slope (°)	Nasal/Superior	11.15 (2.52)	12.92 (2.68)	10.97 (2.57)	12.21 (2.69)	11.40 (2.54)	13.46 (2.79)
	Temporal/Inferior	10.19 (2.55)	12.51 (2.85)	9.99 (2.53)	11.81 (2.69)	10.46 (2.53)	13.05 (2.80)

The columns under All are for all eyes. The columns under Round Bottom are for eyes with round pit bottoms (bottom width ≤ 30 μm). The columns under Flat Bottom are for eyes with flat pit bottoms (bottom width > 30 μm). For the Nasal/Superior location, the numbers in the Horizontal columns are on the Nasal side of the pit and those in the Vertical columns are on the Superior side. Similarly, for the Temporal/Inferior location, the numbers in the Horizontal columns are on the Temporal side of the pit and those in the Vertical columns are on the Inferior side.

Table 2.

Repeatability of foveal pit parameters determined by a Sloped Piecemeal Gaussian fit to 1140 eyes with three good scans. Intra-session standard deviation (mean of standard deviations of repeated measures), shown in absolute values and in percentages of the means

	Intra-session standard deviation	
Pit parameters	**Absolute value**	**Percentage**
Maximum thickness (μm)	6.1	1.89
Minimum thickness (μm)	5.5	2.68
Mean pit depth (μm)	6.7	6.19
Wall slope (°)	1.20	8.26
Top pit width (μm)	132.1	6.45
Mid pit width (μm)	45.9	6.36